Classification
Physics Abstracts
64.60 — 82.70

Three interacting strings in two dimensions: non-universal and multiple unbinding transitions

Roland R. Netz and Reinhard Lipowsky

Institut für Festkörperforschung, Forschungszentrum Jülich, 52425 Jülich, Germany

(Received 26 July 1993, accepted 8 October 1993)

Abstract. — Three non-intersecting strings in two dimensions which interact via short-ranged attractive potentials are studied using both transfer matrix methods and Monte Carlo techniques. The critical behavior at the unbinding transition and the critical values of the potential strength are determined for symmetric and asymmetric bundles of strings. In the asymmetric case, for which the two outer strings have different line tensions (or interact via different potentials), the strings unbind in two subsequent transitions, which then exhibit universal critical behavior. In the symmetric case, where the two outer strings have the same line tension, the three strings unbind simultaneously. The critical behavior at this unbinding transition is found to be non-universal for the whole range of accessible length scales, but its parameter dependence is found to be in strong disagreement with the predictions of the so-called necklace model. The more flexible the inner string, the deeper the critical potential. However, within the numerical error, three identical strings are found to unbind at the same critical potential strength as two strings with the same line tensions.

1. Introduction.

In general, low-dimensional manifolds which interact via short-ranged attractive potentials and which cannot intersect have been shown, both experimentally and theoretically, to undergo unbinding transitions. At low temperatures (or large attractive potentials) the manifolds are tightly bound together, thereby minimizing the internal energy. At sufficiently elevated temperatures (or sufficiently weakened potentials) the manifolds are unbound, maximizing entropy by sampling a larger portion of configuration space. In between, an unbinding transition takes place [1]. Experimental realizations comprise wetting transitions of interfaces in two or three dimensions [2] and adhesion transitions of membranes [3, 4]. In this paper, we address the unbinding behavior of three strings in two dimensions. The term "string" refers to a one-dimensional line which (i) is directed (and exhibits an average orientation of its tangent vectors) and (ii) is governed by a finite line tension. Physical examples are domain walls in adsorbed monolayers, steps on vicinal surfaces, and stretched polymers on a surface.

The unbinding of three interacting strings was first discussed in the context of the so-called necklace model [5]. In this model, one considers a limited set of configurations in which the strings form two types of segments: within these segments, they either form bound triplets or are completely unbound. The segments are connected via '3-body collisions' at which three strings bind or unbind simultaneously. This model neglects all configurations in which two strings form a bound pair to which the third string does not adhere and, thus, all '2-body collisions' between two single strings or between a single string and a bound pair of strings.

On the other hand, one would expect that 2-body collisions are more frequent than 3-body collisions and thus should be important for the unbinding behavior. Indeed, if 3-body collisions were exceptional configurations, one would even expect that the critical behavior is dominated by bound pairs and 2-body collisions.

We have found that the latter behavior does indeed apply to the *asymmetric* case in which the two outer strings have a different stiffness (or are subject to different pair potentials). In this case, a sequence of two unbinding transitions has been found which are governed by 2-body collisions and thus exhibit universal critical exponents.

The *symmetric* case in which the two outer strings have the same stiffness and interact with identical pair potentials turns out to be more subtle. This case was first studied in the analogous context of fluid membranes [6]. Monte Carlo studies of a symmetric bunch of these membranes showed an unbinding critical behavior which was clearly different from the case of two membranes [7]. The effective critical exponents which were extracted from these simulations were different both from the critical exponents for two membranes and from the corresponding exponents for the necklace model.

Much more accurate data can be obtained by numerical transfer matrix calculations for three strings in two dimensions. As has been previously reported in a short paper, the transfer matrix calculations yield data which scale rather accurately over the accessible parameter range [8]. The transfer matrix data clearly indicate a continuous unbinding transition whereas the necklace model predicts a discontinuous one. However, the effective critical exponents extracted from these data are again different from the case of two strings and exhibit a nonuniversal parameter dependence.

This nonuniversal behavior can be understood in a heuristic way if one considers the configurations of three strings which form two bound triplets at their edges. In such a situation, the string in the middle is confined by the two outer strings and will experience a loss of entropy which scales as $\sim 1/l^2$ with the separation l of the two outer strings [1]. This entropy loss would lead to an effective repulsive interaction between the two outer strings. It has been well-established that the critical behavior of two strings with an interaction $\approx W/l^2$ is nonuniversal and exhibits critical exponents which depend on W [1]. As shown below, our transfer matrix calculations imply that such an entropic force acts over the accessible range of separations.

On the other hand, there are now several results which indicate that, on sufficiently large scales, the asymptotic critical behavior might still be universal. Universal behavior has been found within two mean-field theories [9, 10] and from an approximate mapping of the string problem to a quantum spin chain [11]. In addition, the Schrödinger equation which corresponds to N identical strings has been solved in the limit of infinitesimally small potential range which again yields universal behavior [12]. This would imply that the effective repulsion becomes short-ranged at some sufficiently large scale. So far, our transfer matrix calculations show no indication of such a crossover scale.

The paper is organized as follows. The effective Hamiltonian for three interacting strings is defined in section 2 after a brief review of the two-string behavior. The statistical properties of this model can be studied by transfer matrix methods as explained in subsection 2.3. This leads to another representation of the necklace model. However, this model represents a rather

crude approximation to the problem considered here since even the exactly known limiting case of a hard wall sandwiched by two flexible strings is poorly described, as shown in section 3. In general, one has to discretize the transfer matrix in order to perform numerical iterations, see section 4. Transfer matrix results for the symmetric and the asymmetric case are presented in sections 5 and 7, respectively; section 6 contains the Monte Carlo results for the symmetric case. Due to renormalization-group arguments along the same lines as those given in reference [1], our results for three strings in *two* dimensions should also apply to the unbinding of three fluid membranes in *three* dimensions, see section 8.

2. Continuum models for strings.

2.1 BEHAVIOR OF TWO INTERACTING STRINGS. — The interaction of two strings can be described by the effective Hamiltonian[1]

$$\mathcal{H}\{l_1, l_2\} = \int \mathrm{d}x \left\{ \frac{1}{2} K_1 \left(\frac{\mathrm{d}l_1(x)}{\mathrm{d}x} \right)^2 + \frac{1}{2} K_2 \left(\frac{\mathrm{d}l_2(x)}{\mathrm{d}x} \right)^2 + V(l_1(x) - l_2(x)) \right\}. \tag{1}$$

The strings are assumed to be, on average, parallel to each other. Their configurations are then determined by scalar, single-valued functions $l_1(x)$ and $l_2(x)$. The interaction potential contains a hard wall at zero separation (i.e., the strings can not penetrate) and falls off to zero for large separation. The parameters K_1 and K_2 denote the line stiffness. Since the interaction potential is taken to depend only on the local separation $l(x) \equiv l_1(x) - l_2(x)$ of the strings (which is perpendicular to the average tangent vector), we can extract the center of mass coordinate and obtain the effective Hamiltonian

$$\mathcal{H}\{l\} = \int \mathrm{d}x \left\{ \frac{1}{2} K \left(\frac{\mathrm{d}l(x)}{\mathrm{d}x} \right)^2 + V(l(x)) \right\} \tag{2}$$

for the local separation l, with $K \equiv K_1 K_2/(K_1 + K_2)$. This problem can be solved exactly, and four different scaling regimes for general interaction potentials can be identified [1]. These four regimes are distinguished by the functional form of the long-ranged part of the potential and arise due to the competition of the external potential with the fluctuation-induced repulsion between two strings. The latter, effective interaction goes as

$$V_{\mathrm{FL}} \sim 1/l^2. \tag{3}$$

If $V(l) \gg 1/l^2$ for large l, one is either in the *mean-field* regime or in the *weak-fluctuation* regime. The weak-fluctuation regime is defined by $V_{\mathrm{R}}(l) \ll 1/l^2 \ll V_{\mathrm{A}}(l)$, where V_{R} and V_{A} denote the repulsive and attractive parts of the interaction, respectively; the mean-field regime is defined by $1/l^2 \ll V_{\mathrm{R}}(l) \ll V_{\mathrm{A}}(l)$. The case $V(l) \ll 1/l^2$ constitutes the *strong-fluctuation* regime, and the so-called *intermediate* regime is characterized by $V(l) \sim 1/l^2$, which again contains three subregimes with complex critical behavior [13]. The latter regime, where the external potential has the same functional form as the fluctuation-induced interaction, is characterized by non-universal unbinding transitions, with critical behavior depending on the amplitude of the external potential.

A renormalization-group treatment of the corresponding problem for two fluid membranes leads to identical fixed point structures [1]. The unbinding transitions of interfaces in two dimensions and membranes in three dimension should therefore proceed analogously, as indeed confirmed by Monte-Carlo simulations [7].

2.2 EFFECTIVE HAMILTONIAN FOR THREE INTERACTING STRINGS. — To proceed, consider three strings in a plane which are, on average, parallel to each other. Their tensions are denoted by K_1, K_2, and K_3, and their mutual interactions by $V_{12}(l_1 - l_2)$ and $V_{23}(l_2 - l_3)$, which are taken to depend only on their local distances. Interactions are restricted to nearest neighbors only; the effect of further-nearest neighbor interactions will be discussed elsewhere. In the remainder of this work, we are concerned with interactions of the square-well form:

$$\begin{aligned} V_{ij}(l) &= \infty && \text{for } l < 0 \\ &= V_{ij}^{\circ} && \text{for } 0 < l < l_{ij}^{\circ} \\ &= 0 && \text{for } l_{ij}^{\circ} < l \end{aligned} \tag{4}$$

with $(i,j) = (1,2)$ and $(2,3)$. Attractive potentials correspond to V_{12}° and $V_{23}^{\circ} < 0$. Clearly, within the classification scheme presented above, a square-well potential belongs to the strong-fluctuation regime in the case of two strings.

The effective Hamiltonian for the three strings is then given by

$$\begin{aligned} \mathcal{H}\{l_1, l_2, l_3\} = \int \mathrm{d}x \Bigg\{ & \frac{K_1}{2}\left(\frac{\mathrm{d}l_1}{\mathrm{d}x}\right)^2 + \frac{K_2}{2}\left(\frac{\mathrm{d}l_2}{\mathrm{d}x}\right)^2 + \frac{K_3}{2}\left(\frac{\mathrm{d}l_3}{\mathrm{d}x}\right)^2 \\ & + V_{12}(l_1 - l_2) + V_{23}(l_2 - l_3)\Bigg\}. \end{aligned} \tag{5}$$

The Hamiltonian can be substantially simplified by making an orthogonal transformation [14, 5, 6] to extract the center of mass coordinate, which then diffuses freely (see Appendix A). The Hamiltonian for the relative displacement fields then has the form

$$\begin{aligned} \mathcal{H}\{y_1, y_2\} = \int \mathrm{d}x \Bigg\{ & \frac{1}{2}\left(\frac{\mathrm{d}y_1}{\mathrm{d}x}\right)^2 + \frac{1}{2}\left(\frac{\mathrm{d}y_2}{\mathrm{d}x}\right)^2 + V_{12}\left(\sqrt{\frac{1}{K_1} + \frac{1}{K_2}}\, y_1\right) \\ & + V_{23}\left(\sqrt{\frac{1}{K_2} + \frac{1}{K_3}}\,(y_2 \sin\theta - y_1 \cos\theta)\right)\Bigg\} \end{aligned} \tag{6}$$

with

$$y_1 = \left(\frac{K_1 K_2}{K_1 + K_2}\right)^{1/2} (l_1 - l_2) \tag{7}$$

and

$$y_2 = \left(\frac{(K_1 + K_2)K_3}{K_1 + K_2 + K_3}\right)^{1/2} \left[\frac{K_1}{K_1 + K_2}(l_1 - l_2) + l_2 - l_3\right], \tag{8}$$

where the center of mass coordinate y_3 has been omitted already. The hard wall at $l_1 = l_2$ corresponds to $y_1 = 0$; the one at $l_2 = l_3$ to $y_1 = [K_2(K_1 + K_2 + K_3)/K_1 K_3]^{1/2} y_2$, see figure 1.

Using the ratios of the line tensions, which are denoted by

$$q_1 \equiv K_1/K_2 \quad \text{and} \quad q_3 \equiv K_3/K_2, \tag{9}$$

the angle θ is given by

$$\theta = \arctan(\sqrt{1/q_1 + 1/q_1 q_3 + 1/q_3}). \tag{10}$$

The problem of three strings in a two-dimensional plane with mutual square-well interactions has thus been transformed to a problem of one string in a three-dimensional wedge with the square-well potential at its surface, as shown in figure 1. For the transformed system as shown in the right part of figure 1, one distinguishes four regions of different potential depths, denoted

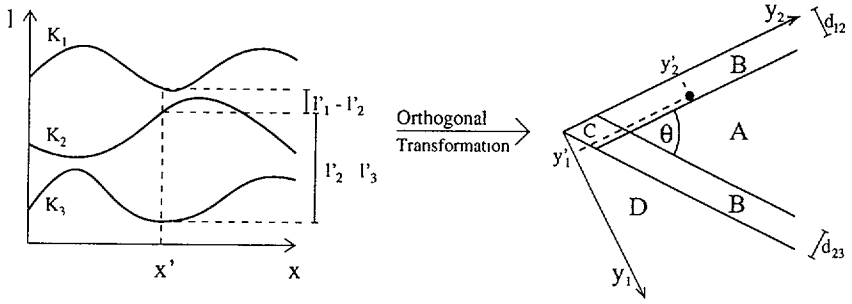

Fig. 1. — Visualization of the orthogonal transformation. The problem of three strings with arbitrary line tensions in two dimensions (to the left), interacting with square well potentials, is transformed into the problem of one string in a three-dimensional wedge with angle θ and square-well potentials of width d_{12} and d_{23} at the boundaries. Here a slice of the wedge at $x = x'$ with the distances $l'_1 - l'_2 = (1/K_1 + 1/K_3)^{1/2} y'_1$ and $l'_2 - l'_3 = (1/K_2 + 1/K_3)^{1/2}(y'_2 \sin\theta - y'_1 \cos\theta)$ is shown.

by A, B, C, and D: they correspond to zero potential, potential depth $-V^{\circ}_{12}$ or $-V^{\circ}_{23}$, potential depth $-V^{\circ}_{12} - V^{\circ}_{23}$, and infinitely high potential, respectively. The thickness of the two strips denoted by B in the (y_1, y_2)-plane can be read off from (6) and is given by

$$d_{12} = \sqrt{\frac{K_1 K_2}{K_1 + K_2}}\, l^{\circ}_{12} = \sqrt{K_1/(1+q_1)}\, l^{\circ}_{12} \tag{11}$$

and

$$d_{23} = \sqrt{\frac{K_2 K_3}{K_2 + K_3}}\, l^{\circ}_{23} = \sqrt{K_3/(1+q_3)}\, l^{\circ}_{23}. \tag{12}$$

The ratio of the thicknesses is given by

$$\frac{d_{12}}{d_{23}} = \sqrt{\frac{q_1(q_3+1)}{q_3(q_1+1)}}\, \frac{l^{\circ}_{12}}{l^{\circ}_{23}}. \tag{13}$$

The string is on average parallel to the corner of the wedge; in figure 1 we demonstrate the transformation for one particular value x' of the x-coordinate.

For the symmetric case, with $K_1 = K_3$, the angle of the wedge is given by

$$\theta = \arctan(\sqrt{2/q + 1/q^2}), \tag{14}$$

where

$$q \equiv q_1 = q_3 \tag{15}$$

and $q = (1 + \sqrt{1 + \tan^2\theta})/\tan^2\theta$. For $q = 0$ we get $\theta = \pi/2$ and the Hamiltonian decouples into two independent problems, each of which can be solved exactly. For $q = 1$ we get $\theta = \pi/3$; as q becomes larger and the inner string becomes more flexible, the angle θ of the wedge decreases.

2.3 TRANSFER MATRIX FOR CONTINUUM MODEL. — Since x is a one-dimensional coordinate (which plays the role of time), the statistical properties of the model defined by the Hamiltonian

(6) can be studied by transfer matrix methods [15, 16] which lead to a two-dimensional time-independent Schrödinger-type equation

$$\hat{H}\Psi_n(y_1, y_2) = E_n\Psi_n(y_1, y_2), \tag{16}$$

with the Hamilton operator

$$\hat{H} = -\frac{T^2}{2}\left(\frac{\partial^2}{\partial y_1^2} + \frac{\partial^2}{\partial y_2^2}\right) + V_{12}\left(\sqrt{\frac{1}{K_1} + \frac{1}{K_2}}\, y_1\right) + V_{23}\left(\sqrt{\frac{1}{K_2} + \frac{1}{K_3}}(y_2 \sin\theta - y_1 \cos\theta)\right), \tag{17}$$

which describes a 'quantum-mechanical' particle in a two-dimensional potential of the form given in figure 1.

First, it is convenient to rescale the coordinate system in such a way that the sum of the widths of the potential strips equals two rescaled units. Using the expressions (11) and (12) for the thicknesses one chooses

$$\bar{y_1} = 2y_1/(d_{12} + d_{23}) \quad \text{and} \quad \bar{y_2} = 2y_2/(d_{12} + d_{23}). \tag{18}$$

Using Equations (11) through (13) one finds the Hamilton operator in the new coordinates to be given by

$$\begin{aligned} \hat{H} \;=\; & -\frac{2T^2}{(d_{12} + d_{23})^2}\left(\frac{\partial^2}{\partial \bar{y}_1^2} + \frac{\partial^2}{\partial \bar{y}_2^2}\right) + V_{12}\left(\frac{l_{12}^{\circ}(d_{12} + d_{23})}{2d_{12}}\bar{y}_1\right) \\ & + V_{23}\left(\frac{l_{23}^{\circ}(d_{12} + d_{23})}{2d_{23}}(\bar{y}_2 \sin\theta - \bar{y}_1 \cos\theta)\right). \end{aligned} \tag{19}$$

By introducing rescaled potentials

$$v_{12}(\bar{y}_1) \equiv \frac{(d_{12} + d_{23})^2}{2T^2} V_{12}\left(\frac{l_{12}^{\circ}(d_{12} + d_{23})}{2d_{12}}\bar{y}_1\right) \tag{20}$$

and

$$v_{23}(\bar{y}_3) \equiv \frac{(d_{12} + d_{23})^2}{2T^2} V_{23}\left(\frac{l_{23}^{\circ}(d_{12} + d_{23})}{2d_{12}}\bar{y}_3\right), \tag{21}$$

which have the same potential range $2d_{12}/(d_{12} + d_{23})$, and the rescaled energy

$$\epsilon_n \equiv \frac{(d_{12} + d_{23})^2}{2T^2} E_n, \tag{22}$$

one can eliminate all prefactors and obtains the Schrödinger-type equation

$$\hat{H}\Psi_n(\bar{y}_1, \bar{y}_2) = \epsilon_n\Psi_n(\bar{y}_1, \bar{y}_2), \tag{23}$$

with the Hamilton operator

$$\hat{H} = -\left(\frac{\partial^2}{\partial \bar{y}_1^2} + \frac{\partial^2}{\partial \bar{y}_2^2}\right) + v_{12}(\bar{y}_1) + v_{23}\left(\frac{d_{12}}{d_{23}}(\bar{y}_2 \sin\theta - \bar{y}_1 \cos\theta)\right). \tag{24}$$

Within the $(\bar{y}_1, \bar{y}_2)$-plane, the range of the two potential wells is given by $2d_{12}/(d_{12} + d_{23})$ and $2d_{23}/(d_{12} + d_{23})$, respectively.

Using the latter form of the problem, three different cases can be distinguished:
(A), the general asymmetric case which is characterized by the angle $\theta = \theta(q_1, q_3)$ as given by (10) and by three additional parameters, namely (i) $v_{12} = -(d_{12} + d_{23})^2 V_{12}^\circ / 2T^2$; (ii) $v_{23} = -(d_{12} + d_{23})^2 V_{23}^\circ / 2T^2$; and (iii) d_{12}/d_{23};
(B), the restricted asymmetric case with

$$V^\circ \equiv V_{12}^\circ = V_{23}^\circ, \tag{25}$$

leading to two parameters besides the angle θ, namely (i) $v \equiv v_{12} = v_{23} = -(d_{12}+d_{23})^2 V^\circ / 2T^2$ and (ii) d_{12}/d_{23}; and
(C), the symmetric case with $V^\circ \equiv V_{12}^\circ = V_{23}^\circ$ and

$$d \equiv d_{12} = d_{23} \tag{26}$$

which depends on θ and only one additional parameter, namely $v = -2d^2 V^\circ / T^2$. For the cases (B) and (C), the rescaled temperature is taken to be

$$t \equiv \sqrt{1/v}. \tag{27}$$

In the following, we will focus on case (B) which includes the symmetric case (C). The latter case (C) does not only apply to $q_1 = q_3$ and $l_{12}^\circ = l_{23}^\circ$, but to the more general situation with

$$\sqrt{q_1/(1+q_1)}\, l_{12}^\circ = \sqrt{q_3/(1+q_3)}\, l_{23}^\circ, \tag{28}$$

as follows from (13).

For the case $K_2 = \infty$, i.e., if the middle string is a hard wall, one obtains

$$\theta = \pi/2 \quad \text{and} \quad \frac{d_{12}}{d_{23}} = \frac{l_{12}^\circ}{l_{23}^\circ} \sqrt{\frac{K_1}{K_3}}. \tag{29}$$

In all of these cases, it is worth noticing that a difference in the range of the two potential wells of the Hamilton operator (24) arises even if the ranges of the original potentials l_{12}° and l_{23}° are equal, due to a difference in the tension ratios q_1 and q_3, compare (13).

3. Necklace model.

In this section we will consider an approximation to the two-dimensional potential in (17) which leads to another representation of the necklace model. This gives rise to a long-ranged repulsive potential between the two outer strings due to the presence of the inner string.

As already mentioned in the Introduction, one distinguishes in the necklace model only between segments of the string system in which all strings are bound together, and segments where all strings are separated; these are the strands and beads of the 'necklace', and they can alternate in an arbitrary fashion. Within the context of the two-dimensional Schrödinger equation, the approximation used in the necklace model consists of changing the pair potential $V(l)$ between nearest-neighbor strings into a merely repulsive one, as given by

$$\begin{aligned} \tilde{V}(l) \quad &= \infty \qquad \text{for } l < 0 \\ &= 0 \qquad \text{for } 0 < l. \end{aligned} \tag{30}$$

Thus, the steric part of the interaction is treated exactly. The attraction between the strings is accounted for in an approximate fashion by keeping an attractive contact potential solely

between the two outer strings, which can be thought of as a very short-ranged potential of depth P_o, expressed as $P(y_1, y_2)$, which is centered around the corner of the wedge. If the two outer strings are bound together, which means that all three strings form a bound state, the system gains an energy P_o. On the other hand, if the two outer strings are separated (which does not necessarily mean that all strings are separated), the total attractive energy gain is taken to be zero.

The Hamilton operator corresponding to the necklace model is thus given by

$$\begin{aligned}\hat{H} &= -\frac{T^2}{2}\left(\frac{\partial^2}{\partial y_1^2}+\frac{\partial^2}{\partial y_2^2}\right)+\tilde{V}\left(\sqrt{\frac{1}{K_1}+\frac{1}{K_2}}\,y_1\right)\\ &\quad+\tilde{V}\left(\sqrt{\frac{1}{K_2}+\frac{1}{K_3}}\,(y_2\sin\theta-y_1\cos\theta)\right)+P(y_1,y_2),\end{aligned} \tag{31}$$

which describes a particle in a two-dimensional potential angle with infinitely high walls and an attractive region in the corner. The angle θ is again given by (10).

The corresponding Schrödinger-type equation can be separated in polar coordinates r and ϑ, if the contact potential $P(y_1, y_2)$ is taken to be radially symmetric, i.e., $P(y_1, y_2) \equiv \tilde{P}(r)$. Then, the potential walls embodied in $\tilde{V}(l)$ lead to a boundary condition for $\vartheta = 0$ and $\vartheta = \theta$, and we get

$$\left\{-(T^2/2)\left(\partial^2/\partial r^2+(1/r)\partial/\partial r+(1/r^2)\partial^2/\partial\vartheta^2\right)+\tilde{P}(r)\right\}\Psi_n(r,\vartheta)=E_n\Psi_n(r,\vartheta), \tag{32}$$

with

$$\Psi_n(r,0)=\Psi_n(r,\theta)=0. \tag{33}$$

The attractive potential $\tilde{P}(r)$ is defined by

$$\begin{aligned}\tilde{P}(r) &= P_o \quad \text{for } 0<r<r_o\\ &= 0 \quad \text{for } r_o<r,\end{aligned} \tag{34}$$

with $P_o < 0$.

Due to the boundary conditions (33), the solution has to be of the form

$$\Psi_n(r,\vartheta)=\psi_n(r)\sin(l\pi\vartheta/\theta)\equiv r^{-1/2}\Phi_n(r)\sin(l\pi\vartheta/\theta), \tag{35}$$

where l is an integer. This leads to

$$\left\{-(T^2/2)\left(\mathrm{d}^2/\mathrm{d}r^2+(1/4-(l\pi/\theta)^2)/r^2\right)+\tilde{P}(r)\right\}\Phi_n(r)=E_n\Phi_n(r). \tag{36}$$

Introducing the rescaled coordinate $z \equiv r/r_o$ we obtain finally

$$\left\{-\mathrm{d}^2/\mathrm{d}z^2+w/z^2+\tilde{p}(z)\right\}\phi_n(z)=\varepsilon_n\phi_n(z), \tag{37}$$

with $\phi_n(r/r_o) \equiv \Phi_n(r)$, $\varepsilon_n \equiv 2r_o^2E_n/T^2$, and $w \equiv (l\pi/\theta)^2 - 1/4$. The rescaled potential $\tilde{p}$ is given by

$$\begin{aligned}\tilde{p}(z) &= p_o \quad \text{for } 0<z<1\\ &= 0 \quad \text{for } 1<z\end{aligned} \tag{38}$$

with $p_o \equiv 2r_o^2 P_o/T^2$,

The ground state is obtained for $l = 1$, which implies that the long-range potential has the amplitude [17]

$$w = \pi^2/\theta^2 - 1/4. \tag{39}$$

Thus, the necklace model gives an effective repulsive potential which goes as $1/z^2 \sim 1/r^2$, in agreement with the simple scaling picture. As mentioned above, the corresponding critical unbinding behavior belongs to the intermediate fluctuation regime. This problem has been solved in [13] with the following results:

First one defines the length scales

$$\xi_m \equiv \langle (z - \langle z \rangle)^m \rangle^{1/m}, \tag{40}$$

where m is taken to be positive and real. The interfacial roughness is given by $\xi_\perp = \xi_2$. The unbinding transition occurs at a rescaled potential depth $p_o = p_c$. Now the following subregimes can be distinguished.

For subregime (B) with $-1/4 < w < 3/4$ one gets non-universal critical behavior with a parallel correlation length which governs the exponential decay of correlations parallel to the strings and which diverges as

$$\xi_\parallel \sim 1/\varepsilon_0 \sim (p_c - p_o)^{-\nu_\parallel}, \tag{41}$$

where ε_0 is the ground state energy and

$$\nu_\parallel = (1/4 + w)^{-1/2} = \theta/\pi. \tag{42}$$

In this regime, all length scales satisfy the scaling relation

$$\langle z \rangle \sim \xi_\perp \sim \xi_\parallel^\zeta \tag{43}$$

with $\zeta = 1/2$.

For subregime (C) with $w > 3/4$, one has $\nu_\parallel = 1$ but

$$\xi_m \sim (p_c - p_o)^{-\nu_m} \tag{44}$$

with

$$\nu_m = \frac{1}{m}\left(\frac{m+2}{2} - (1/4 + w)^{1/2}\right) = \frac{1}{m}\left(\frac{m+2}{2} - \frac{\pi}{\theta}\right) \tag{45}$$

for $m > (1 + 4w)^{1/2} - 2 = 2(\pi/\theta - 1) > 0$.

Our way of solving the necklace model leads to exactly the same results as the original solution [5, 18], but in addition we obtain the effective potential in an explicit form, see (39). The amplitude w of the repulsive potential vanishes for $\theta = 2\pi$, which is not realizable within the original model as given by (17). The smallest value obtainable from this model is $w = 15/4$ for $\theta = \pi/2$, which corresponds to the case of two strings separated by a rigid wall. In this case, the original model can be solved exactly and gives $w = 0$. The value of w obtained within the necklace model is rather high and leads already to a strongly discontinuous unbinding transition. The presence of such a strongly repulsive potential even for the case of two decoupled strings is an artefact of the necklace model in which attractive nearest-neighbor interactions have been omitted.

Another severe limitation of the necklace model is that the successive unbinding of the three strings at two different transition points is excluded *a priori*. As is shown below, the strings actually do undergo two unbinding transitions as soon as one has two different potential ranges $d_{12} \neq d_{23}$.

One way of improving upon the result within the framework of the necklace model consists in changing the boundary condition along the edges of the wedge in such a way, that one recovers the exact result for $\theta = \pi/2$. This amounts to the shifted angle $\theta' = \theta + 3\pi/2$ as the new angle of the wedge, where θ is still given by (10). The resulting amplitude is

$$w = (\pi/\theta')^2 - 1/4 = \pi^2/(\theta + 3\pi/2)^2 - 1/4 \tag{46}$$

which leads to

$$\nu_{\|} = \theta/\pi + 3/2. \tag{47}$$

As will be shown below, this gives a good fit to the critical behavior at and near $\theta = \pi/2$.

4. Transfer matrix for the discretized model.

Here, we introduce the numerical transfer matrix method. For the application of this formalism, the spatial coordinate x will be discretized into a lattice with sites $\{x_i\}$ and lattice constant Δx. The string configuration is then specified by $y_{\alpha i} \equiv y_\alpha(x_i)$ $(\alpha = 1, 2)$, and the Hamiltonian (6) now takes the form

$$\begin{aligned}\mathcal{H}\{y_{1i}, y_{2i}\} &= \sum_i \Delta x \left\{ \frac{1}{2}\frac{(y_{1i} - y_{1i+1})^2}{\Delta x^2} + \frac{1}{2}\frac{(y_{2i} - y_{2i+1})^2}{\Delta x^2} + V_{12}\left(\sqrt{\frac{1}{K_1} + \frac{1}{K_2}}\, y_{1i}\right)\right. \\ &\left. + V_{23}\left(\sqrt{\frac{1}{K_2} + \frac{1}{K_3}}\,(y_{2i}\sin\theta - y_{1i}\cos\theta)\right)\right\}. \end{aligned} \tag{48}$$

Now we decompose this discretized Hamiltonian as

$$\mathcal{H}\{z_{1i}, z_{2i}\}/T = \sum_i H_i(z_{1i}, z_{2i}, z_{1i+1}, z_{2i+1}), \tag{49}$$

with

$$\begin{aligned} H_i(z_{1i}, z_{2i}, z_{1i+1}, z_{2i+1}) &= \frac{1}{2}(z_{1i} - z_{1i+1})^2 + \frac{1}{2}(z_{2i} - z_{2i+1})^2 + \hat{V}_{12}(z_{1i+1}) \\ &+ \hat{V}_{23}(z_{2i+1}\sin\theta - z_{1i+1}\cos\theta), \end{aligned} \tag{50}$$

where we have used the rescaled variables $z_{\alpha i} \equiv y_{\alpha i}/\sqrt{\Delta x T}$ and the reduced interactions $\hat{V}_{12}(z) \equiv \Delta x V_{12}(\sqrt{\Delta x T(K_1 + K_2)/K_1 K_2}\, z)/T$ and $\hat{V}_{23}(z) \equiv \Delta x V_{23}(\sqrt{\Delta x T(K_2 + K_3)/K_2 K_3}\, z)/T$. The potential depths of these reduced interactions are given by

$$\hat{V}_{12}(z) = -U_{12} \equiv \frac{\Delta x}{T} V_{12}^\circ \quad \text{for} \quad 0 < z < z_{12}^\circ \tag{51}$$

and

$$\hat{V}_{23}(z) = -U_{23} \equiv \frac{\Delta x}{T} V_{23}^\circ \quad \text{for} \quad 0 < z < z_{23}^\circ \tag{52}$$

with the potential ranges given by

$$z_{12}^\circ \equiv \frac{d_{12}}{\sqrt{\Delta x T}} \quad \text{and} \quad z_{23}^\circ \equiv \frac{d_{23}}{\sqrt{\Delta x T}}. \tag{53}$$

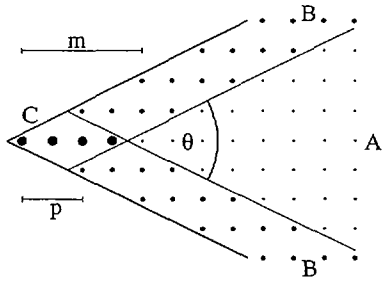

Fig. 2. — Discretization of the wedge for $q = K_1/K_2 = K_3/K_2 = 1.5$, or $\theta = 2\arctan(1/2)$, as used in the transfer matrix calculation. The potential depths in the regions denoted by A, B, and C are $0, U$, and $2U$, respectively.

The statistical weight $W(z_{1i+1}, z_{2i+1})$ of a path ending at (z_{1i+1}, z_{2i+1}) satisfies the recursion relation

$$W(z_{1i+1}, z_{2i+1}) = \mathcal{N}^{-1} \int\int \mathrm{d}z_{1i}\mathrm{d}z_{2i} \exp\left(-H_i(z_{1i}, z_{2i}, z_{1i+1}, z_{2i+1})\right) W(z_{1i}, z_{2i}), \qquad (54)$$

where $\mathcal{N}$ is a normalization constant. The integral kernel in (54) is called the transfer matrix. In our implementation we also discretized the variables z_{1i} and z_{2i} with sites $\{z_{1i}^j\}$ and $\{z_{2i}^k\}$ and lattice constants $\Delta z_1 = \Delta z_2 \equiv \Delta z$ in the directions perpendicular to the strings, replacing the double integral $\int\int \mathrm{d}z_{1i}\mathrm{d}z_{2i}$ by the double sum $\sum_j \sum_k (\Delta z)^2$. Moreover, we restricted the double sum to nearest neighbors only, yielding the so-called restricted solid-on-solid model. Since our system is homogeneous in the x-direction, we drop the i index and obtain the recursion formula

$$W'(z_1^{j'}, z_2^{k'}) = \mathcal{N}^{-1}(\Delta z)^2 \sum_{j=j'-1}^{j'+1} \sum_{k=k'-1}^{k'+1} \exp\left(-H(z_1^j, z_2^k, z_1^{j'}, z_2^{k'}\right) W(z_1^j, z_2^k) \qquad (55)$$

as used in our calculation. The restriction to nearest neighbors should not change the critical behavior but saves computer time. This is well-established for the case $\theta = \pi/2$. We also confirmed this expectation by numerical analysis of a discretized version of the necklace model for the angles $\theta = \pi$, $\pi/2$, $2\arctan(1/2)$, and $2\arctan(1/3)$, where we indeed find accurate agreement between our measured exponents and the exponents derived in the last section, see subsection 4.3.

We discretized the system using 40,000 or 80,000 sites. The recursion relation (55) was iterated typically 20,000 times for each lattice site using a fully vectorized code.

4.1 DISCRETIZATION. — The discretization of the Hamiltonian (50) in the (z_1, z_2)-plane deserves special attention. First of all, the discretization has to be symmetric with respect to an interchange of the two expressions z_1 and $z_2 \sin\theta - z_1 \cos\theta$ if the original system of three strings is symmetric under an interchange of the outer two strings. This can be achieved by putting the bisector of the potential angle parallel to one of the axes of the orthogonal set of discrete sites $\{z_1^j, z_2^k\}$.

Secondly, the thickness of the square wells has to be chosen in such a way that the density of sites is constant in all regions of the wedge. As an example, consider figure 2 in which the actual realization of the two-dimensional potential for $\theta = 2\arctan(1/2)$ is shown. This is achieved

by displacing the potential edge by $p = 2$ in the horizontal direction at every vertical step. The thickness of the potential in the horizontal direction is denoted by m. The three regions denoted by A, B, C are distinguished by the potential depth being $0, U, 2U$, respectively.

The constants p and m have to be adjusted in such a way that the density of sites in regions B and C are the same. The density d(B) of sites in region B is d(B)= 1 (in units of the lattice constant). The area of region C is $m^2/2\cot(\theta/2)$. The number of sites in region C is (for small enough values of m) equal to m, so the density d(C) is $d(C)$=$2\cot(\theta/2)/m$. Since $\cot(\theta/2) = p$ we arrive at the simple condition $m = 2p$, which is actually met in figure 2. We satisfied this condition for all transfer matrix calculations.

The validity of this discretization is checked by our transfer matrix calculation of the necklace model, presented in subsection 4.3 below.

4.2 OBSERVABLES. — Once the transfer-matrix iteration has been performed sufficiently often, the distribution $W(z_1^j, z_2^k)$ becomes stationary under the operation defined by (55) and we get $W'(\{z_1, z_2\}) = W(\{z_1, z_2\}) \equiv W_{\rm st}(\{z_1, z_2\})$. This stationary state is then proportional to the ground state of the transfer matrix. The expectation value of an operator $A(\{z_1, z_2\})$ for periodic boundary conditions can then be obtained by using

$$\langle A\rangle = \frac{\sum_{j,k} W_{\rm st}^2(z_1^j, z_2^k) A(z_1^j, z_2^k)}{\sum_{j,k} W_{\rm st}^2(z_1^j, z_2^k)} \tag{56}$$

We calculated the mean string separations $\langle l_\alpha\rangle$, and higher moments thereof,

$$\langle l_\alpha^m\rangle^{1/m}, \tag{57}$$

as well as the perpendicular correlation length

$$\xi_\perp^\alpha = \langle (l_\alpha - \langle l_\alpha\rangle)^2\rangle^{1/2}, \tag{58}$$

where the variables l_α are defined by

$$l_{12} \equiv l_1 - l_2 = \sqrt{\frac{\Delta x T(K_1 + K_2)}{K_1 K_2}}\, z_1 \tag{59}$$

and

$$l_{23} \equiv l_2 - l_3 = \sqrt{\frac{\Delta x T(K_2 + K_3)}{K_2 K_3}}\, (z_2 \sin\theta - z_1 \cos\theta). \tag{60}$$

We always checked for the symmetric case $K_1 = K_3$ that the equality $l_{12} = l_{23}$ actually holds. The free energy per unit length can be obtained (up to a constant) via

$$f = -\frac{T \ln \mathcal{N}}{\Delta x} \tag{61}$$

where $\mathcal{N}$ represents the numerically determined normalization as in (55). The parallel correlation length is then given by

$$\xi_\parallel = T/(f_\circ - f), \tag{62}$$

where $f_\circ$ is the free energy of the lowest scattering state (which corresponds to the zero-energy state in the Schrödinger-equation formalism).

In the course of our calculation, we scanned the potential depth $U \equiv U_{12} = U_{23}$ from a large value–where the strings are tightly bound together–to a small value, where one is sufficiently

close to the unbinding transition. We typically calculated the above mentioned averages for 100 values of U, the points distributed logarithmically in U to ensure good fitting in a log-log plot.

We also subtracted from the averages the values at infinitely high potential depth, which can be calculated exactly:

$$\langle l_\alpha \rangle_\infty = l_\alpha^\circ/2 \quad \text{for} \quad U = \infty \tag{63}$$

and

$$\xi_{\perp\infty}^\alpha = l_\alpha^\circ/\sqrt{12} \quad \text{for} \quad U = \infty. \tag{64}$$

These values represent a correction to scaling and are especially important for small values of $\langle l \rangle$. Through the remainder of this paper, these corrections are subtracted from all length scales used for further analysis.

In our transfer matrix calculation (using the Hamiltonian given by (50)) we set the lattice constant Δz equal to one. The line tensions K_1, K_2, and K_3 do not enter the transfer matrix explicitly but determine the wedge angle θ and the ranges z_{12}° and z_{23}° of the potential wells, see (10), (11), (12), and (53).

Another subtle point is the range of the potential depth for which the data are to be considered. If the potential is too deep, the distribution will be centered close to the edge of the wedge and will not feel a continuous angle but rather the single steps of the potential rim (especially for small angles); if the potential is too shallow, the distribution will approach the cutoff of the discretization and the finite size of the system will affect the unbinding.

Calling $l_{\max}$ the maximal value available due to the spatial restriction imposed by the finite system, we obtained data only within the following limits:

$$l_\alpha^\circ \; < \langle l_\alpha \rangle \; < \; l_{\max}/5. \tag{65}$$

Consequently, the data for the discretization introduced in subsection 4.1 are restricted to a range of half a decade in $\langle l \rangle$ or $\xi_\perp$, which seems rather small but nevertheless allowed us to infer effective critical exponents. Furthermore, for $q = 1$, we were able to extend the scaling regime to more than a decade by using a different discretization scheme.

4.3 NUMERICAL TRANSFER MATRIX RESULTS FOR THE NECKLACE MODEL. — The numerical implementation of the transfer matrix method involves two subtle points: (i) the discretization of the wedge for different angles and (ii) the restriction to nearest-neighbors only, the so-called restricted solid-on-solid case. Since the critical behavior is found to be non-universal, i.e., dependent on the model parameters, it is not obvious a priori that this behavior is not affected by (i) and (ii). To check this important point, we performed a numerical transfer matrix calculation of the necklace model, for which the exact exponents were derived in section 3.

The approximation constituting the necklace model is implemented in the numerics by keeping the attractive potential of depth U only on the left two discretization sites of region C in figure 2, having potential zero on all other sites (and similarly for different wedge angles θ). Note that the repulsive part of the potential is treated exactly through the boundary conditions. We performed calculations for $\theta = \pi$, $\pi/2$, $2\arctan(1/2)$, and $2\arctan(1/3)$, the discretization for $\theta = 2\arctan(1/2)$ is shown in figure 2. In figure 3, we show calculated moments of the radial distance from the corner of the wedge, $r \equiv \sqrt{l_{12}^2 + l_{23}^2}$, for the angle $\theta = \pi/2$. The moments were fitted to a power law of the form

$$\langle r^m \rangle^{1/m} \sim (U - U_c)^{-\nu_m} \tag{66}$$

This fit led to the estimate $U_c \simeq 1.35$. The rescaled potential depth, $(U - U_c)/U$, was varied over two orders of magnitudes. The resultant exponents are $\nu_3 = 0.164 \pm 0.005$, $\nu_4 = 0.251 \pm 0.005$,

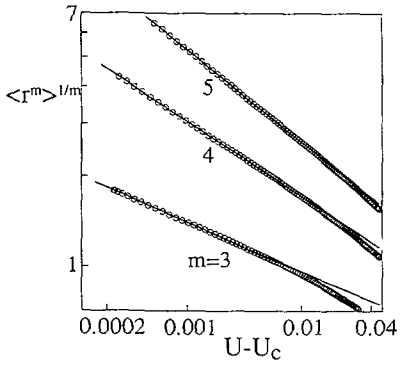

Fig. 3. — Log-log plot of transfer matrix results for the necklace model with $\theta = \pi/2$, corresponding to the middle string being a hard wall.

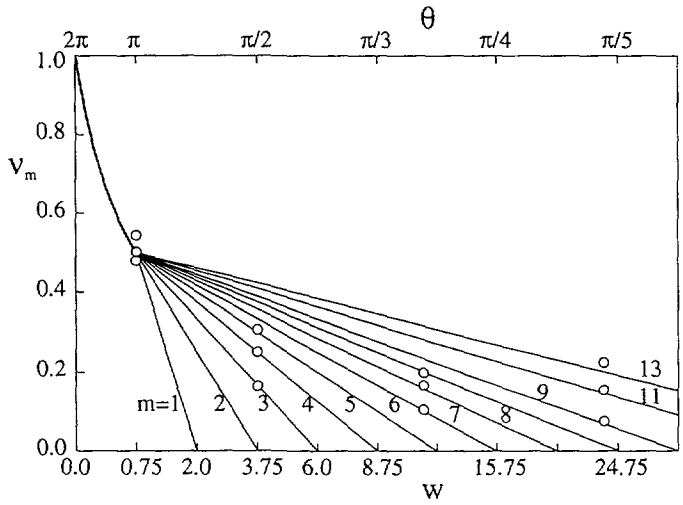

Fig. 4. — Comparison of the analytic results for the necklace model, derived in section 3, and the numerical results for four different angles. Shown are various exponents of the moments of the radial distance, $\langle r^m \rangle^{1/m}$

and $\nu_5 = 0.307 \pm 0.01$, which are to be compared with the analytic results (45) giving $\nu_3 = 1/6$, $\nu_4 = 1/4$, and $\nu_5 = 3/10$. These exponents, together with results for the other wedge angles, are plotted and compared with the exact results in figure 4. The overall agreement between the numerical data and the analytic results is quite satisfactory. Note that for $\theta = \pi$, the border between subregime B (characterized by one length scale), and subregime C (with many different length scales) is reached. In the latter regime, all moments of r scale with a different exponent.

The good agreement shows that (i) the discretization of the wedge is adequate, and (ii) the restricted solid-on-solid approximation does not change the critical behavior. This makes us quite confident about the transfer matrix results obtained and presented in the following.

Table I. — *Symmetric systems with $K_1 = K_3$ as studied by the transfer matrix method with lattice parameter p, wedge angle θ, line tension ratio $q = K_1/K_2$, and width z° of the potential strips in units of the lattice constant Δz. Figure 2 shows the particular discretization used for the third system with $p = 2$, corresponding to the outer strings being 3/2 times more rigid than the middle string. The last column gives the critical potential strength U_c.*

p	wedge angle θ	$q = (p^2-1)/2$	$z^\circ/\Delta z = 2p/(1+p^2)^{1/2}$	U_c
1	$2\arctan(1) = \pi/2$	0	$\sqrt{2}$	0.1930
1.5	$2\arctan(2/3) \simeq 0.37\pi$	0.625	1.6641	0.1543
2	$2\arctan(1/2) \simeq 0.30\pi$	1.5	1.7889	0.1395
3	$2\arctan(1/3) \simeq 0.20\pi$	4	1.8974	0.1273
4	$2\arctan(1/4) \simeq 0.16\pi$	7.5	1.9401	0.1223
6	$2\arctan(1/6) \simeq 0.11\pi$	17.5	1.9723	0.1178
8	$2\arctan(1/8) \simeq 0.08\pi$	31.5	1.9846	0.1158
10	$2\arctan(1/10) \simeq 0.06\pi$	49.5	1.9899	0.1147
12	$2\arctan(1/12) \simeq 0.05\pi$	71.5	1.9937	0.1140

5. Transfer matrix results for symmetric bundles.

For the symmetric case (and in the continuum limit), the critical behavior depends on a single parameter q, defined by $K_1 = qK_2 = K_3$, and the wedge angle $\theta = \arctan\sqrt{2/q + 1/q^2}$ as in (14). For the discretized case, one also expects a nontrivial dependence of non-universal properties (such as the transition temperature) on the small-scale cutoff Δx via the range of the attractive potential $z^\circ \equiv z^\circ_{12} = z^\circ_{23}$ as given by (53). The string separation is now calculated as an average over the two separate string separations

$$\langle l\rangle \equiv \langle l_{12}\rangle/2 + \langle l_{23}\rangle/2, \tag{67}$$

and analogously for the other length scales.

Table I summarizes the parameters of the different symmetric systems studied using the transfer matrix method. The lattice parameter p as given in the first column, determines the angle θ of the wedge and, in turn, the ratio of the line tensions of inner and outer strings. Only a discrete set of angles is accessible using the discretization scheme displayed in figure 2.

5.1 CRITICAL EXPONENTS. — In figures 5 and 6 we show data for the angles $\pi/2$ and $2\arctan(1/8)$, respectively. Here and below, the string separation l is measured in units of the potential range l°. In figures 5a and 6a data for $\langle l\rangle$, $\xi_\perp = \langle (l - \langle l\rangle)^2\rangle^{1/2}$, and $\xi_\parallel = (f_o/T + \ln\mathcal{N})^{-1}$ are plotted on a log-log scale as a function of $U - U_c$, where the corrections to scaling have been subtracted already and U is defined by

$$U \equiv U_{12} = U_{23}, \tag{68}$$

using (51) and (52). First we fitted $\langle l\rangle$ to a straight line in a log-log plot, thus determining U_c and the critical exponent ψ, according to

$$\langle l\rangle \sim (U - U_c)^{-\psi}. \tag{69}$$

The values for the critical exponent $\nu_\perp$ were obtained from fitting $\xi_\perp$ to the form

$$\xi_\perp \sim (U - U_c)^{-\nu_\perp} \tag{70}$$

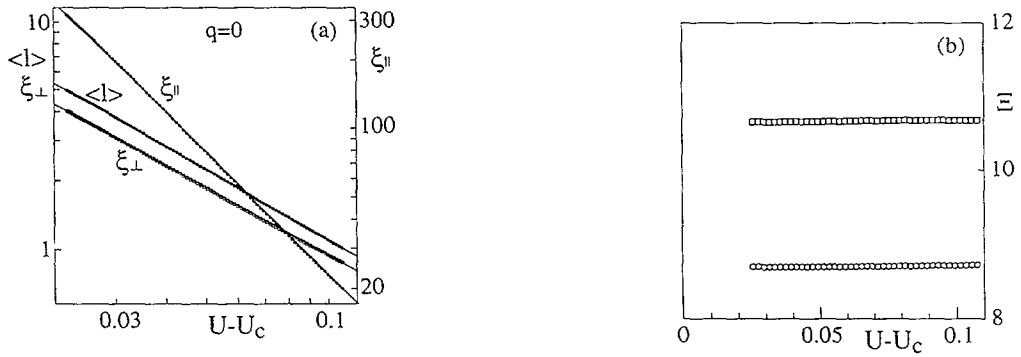

Fig. 5. — Transfer matrix results for the case $K_2 = \infty$ and $K_1 = K_3$, ($q = 0$ and $\theta = \pi/2$). (a) In a log-log plot, data for the parallel correlation length (filled circles) are shown to scale as $\xi_{\|} \sim (U - U_c)^{-\nu_{\|}}$ with $\nu_{\|} = 1.8 \pm 0.2$. The mean separation goes as $\langle l \rangle \sim (U - U_c)^{-\psi}$ with $\psi = 1.01 \pm 0.02$ and the perpendicular correlation length goes as $\xi_{\perp} \sim (U - U_c)^{-\nu_{\perp}}$ with $\nu_{\perp} = 0.99 \pm 0.02$. (b) The difference function Ξ as defined in subsection 5.3 for $\langle l \rangle$ (circles) and $\xi_{\perp}$ (squares) with $\gamma' = 1$.

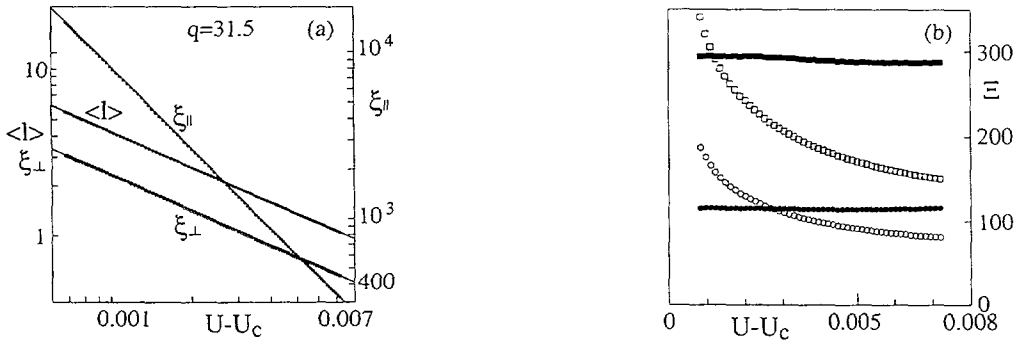

Fig. 6. — Transfer matrix results for the case $K_1/K_2 = K_3/K_2 = 31.5$ or $\theta = 2\arctan(1/8)$. (a) Data for the parallel correlation (filled circles) are shown to scale as $\xi_{\|} \sim (U - U_c)^{-\nu_{\|}}$ with $\nu_{\|} = 1.6 \pm 0.2$. The mean separation behaves as $\langle l \rangle \sim (U - U_c)^{-\psi}$ with $\psi = 0.707 \pm 0.02$ and the perpendicular correlation length diverges as $\xi_{\perp} \sim (U - U_c)^{-\nu_{\perp}}$ with $\nu_{\perp} = 0.712 \pm 0.02$. (b) The difference function Ξ for $\langle l \rangle$ with $\gamma' = 1$ (open circles) and with $\gamma' = 0.707$ (closed circles) and $\xi_{\perp}$ with $\gamma' = 1$ (open squares) and with $\gamma' = 0.712$ (closed squares).

For all fitting procedures we used the Levenberg-Marquardt method for a three-parameter fit [19]. In a second step we fitted $\xi_{\|}$, determining f_o and $\nu_{\|}$.[20] The data for $\langle l \rangle$ and $\xi_{\perp}$ are shown to scale accurately in the same fashion, giving $\psi = 1.01 \pm 0.02$ and $\nu_{\perp} = 0.99 \pm 0.02$ for $\theta = \pi/2$, see figure 5a, and $\psi = 0.71 \pm 0.02$ and $\nu_{\perp} = 0.71 \pm 0.02$ for $\theta = 2\arctan(1/8)$, see figure 6a. The data for $\xi_{\|}$ confirm that the roughness exponent $\zeta = 1/2$ within 5 per cent.

Since there are two fitting procedures involved in determining the behavior of $\xi_{\|}$, this behavior is less reliable than the behavior for $\langle l \rangle$ and $\xi_{\perp}$, and we used the data for the exponents ψ and $\nu_{\perp}$ for further analysis. In figure 7 we plotted the various values for the exponents ψ (open circles) and $\nu_{\perp}$ (filled circles) as a function of the angle θ of the potential wedge. The exactly

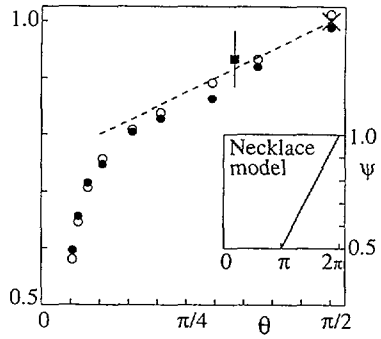

Fig. 7

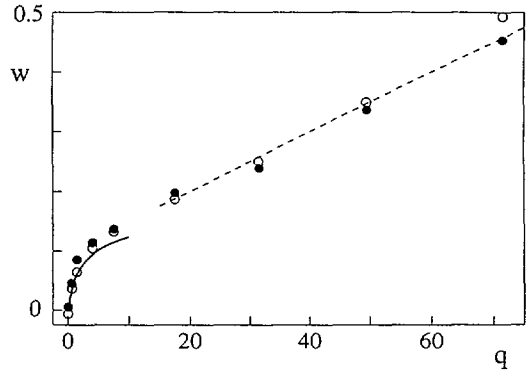

Fig. 8

Fig. 7 — The critical exponents ψ (open symbols) and $\nu_\perp$ (filled symbols) as a function of the wedge angle θ. The square denotes the Monte Carlo result for $\nu_\perp$, the circles denote transfer matrix results. The cross denotes the exactly known result for the case $\theta = \pi/2$, namely $\psi = \nu_\perp = 1$. The prediction of the improved necklace model is shown as a broken line. The inset shows the prediction of the original necklace model, indicating the existence of discontinuous transition for $\theta < \pi$.

Fig. 8. — The effective amplitude w of the fluctuation-induced, repulsive interaction obtained from the results for ψ (open circles) and $\nu_\perp$ (closed circles) as a function of the line tension ratio $q = K_1/K_2 = K_3/K_2$. The prediction of the improved necklace model is shown as a solid line. A linear extrapolation for large q values leads to the prediction $w = 0.75$ (the onset of discontinuous transitions) for $q \simeq 130$.

known result $\psi = 1$ for $\theta = \pi/2$ (denoted by a bold cross) is reproduced quite accurately.

The predictions of the necklace model, which are shown in the inset, are quite different. Following these predictions, subregime (B) with continuous transitions and $\psi > 0.5$ is only realized for $\theta > \pi$. In contrast, we find critical behavior which is characteristic for subregime (B) down to $\theta = 2\arctan(1/12)$, as confirmed by the scaling behavior $\nu_\perp = \psi$.

The results of the improved necklace model, derived in section 3, see (46) and (47), are shown in figure 7 as the broken line; they agree well with our numerical findings for θ close to $\pi/2$.

From the measured exponents we can calculate the amplitude w of the effective repulsive potential, using the expressions $w = 1/(4\psi^2) - 1/4$ and $w = 1/(4\nu_\perp^2) - 1/4$.[13] The resulting data points are shown in figure 8 plotted as a function of the tension ratio q. The results of the improved necklace model are again included and correspond to the solid line. In this plot, the exponents lie approximately on a straight line for large q-values, as indicated by the broken line; extrapolating this line up to $w = 3/4$ corresponding to the onset of the C regime leads to $q \simeq 130$.

Thus, if the critical exponents as determined here govern the asymptotic critical behavior, the line tension of the inner string has to be about 130-times smaller than the tension of the outer strings in order to enter subregime (C), where discontinuous unbinding transitions occur, which are then governed by exceptional fluctuations of the strings. As a consequence, the unbinding of three strings (interacting with short-ranged potentials) will typically proceed via a continuous transition.

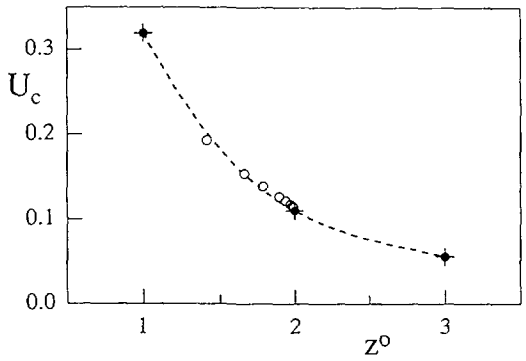

Fig. 9. — Critical potential strength U_c as a function of the potential width z°. Results of the two-dimensional transfer-matrix calculation are shown as open circles, exact results as crosses, and the numerical results of the one-dimensional transfer matrix as filled circles.

5.2 CRITICAL POTENTIAL STRENGTHS. — Another important question, which can be answered using the transfer matrix results, concerns the critical value U_c of the potential depth as a function of the angle θ. In the last column of table I the critical potential strengths are listed. As mentioned above, one expects a nontrivial dependence of the critical potential U_c on the range z° of the potential. In order to separate the effects of the potential range z° and of the wedge angle θ on the critical potential depth, we compare the data for U_c listed in table I with results for the one-dimensional case for $z^\circ = 1, 2$, and 3. As explained in subsection 2.1, the one-dimensional case corresponds to the system of only two strings or one string interacting with a hard wall. It is formally equivalent to the two-dimensional transfer matrix with $\theta = \pi/2$. We solved the discrete one-dimensional system exactly for the three cases considered above (see Appendix B) and obtained very accurate numerical transfer matrix results as well. In figure 9 we show the exact results for U_c (denoted by crosses) together with the numerical results (filled circles), obtained from the one-dimensional transfer matrix for three different values of z°. The agreement between exact and numerical results is very good in this case. The broken line interpolates between these data points. The numerical results of the transfer matrix calculation for the two-dimensional wedge are shown as open circles. The angle decreases monotonically as the potential range z° increases, as determined by our discretizations scheme (see Tab. I). It is observed that the deviations of the two-dimensional results from the interpolation curve are rather small and are probably due to crossover effects. Thus, from a numerical point of view, we could not detect a dependence of the critical potential depth (or the critical temperature via (51) and (52)) on the angle θ. The observed variation in U_c can be explained by the change in z° alone, as suggested by figure 9.

This implies that the unbinding of *two* strings with line tensions K proceeds at the same critical potential strength as the unbinding of *three* strings with identical line tensions K. This can be seen from the fact that, after subtraction of the center-of-mass coordinate, the potential width in the rescaled coordinates is the same for the systems of two and three identical strings and given by (11), (12) and (53) for the continuous and discretized model, respectively. With the result from the last paragraph, we conclude that the critical potential strength U_c does not depend on whether two or three strings unbind. Thus, the unbinding temperature of identical strings seems to be independent of the number of strings involved.

This result seems to stand in contradiction to the scaling picture invoked in the Introduction to explain the observed nonuniversality of the critical exponents. Following the scaling picture,

the presence of a third string between the two outer ones induces an entropically generated effective interaction between the two outer strings which is repulsive and goes like $1/l^2$. Such an interaction should, in fact, increase the critical potential strength.[13] However, this simple argument neglects that the area of the region where all three strings are bound together (region C in Fig. 1) depends on θ and is given by $d_{12}d_{23}/\sin\theta$. For the case of three identical strings ($\theta = \pi/3$), the area of this region is increased by a factor of $2/\sqrt{3} \simeq 1.15$ as compared to the case of two strings ($\theta = \pi/2$). This increase in area of the attractive corner could compensate the effective repulsive interaction and lead to the observed universality in U_c.

A question pertaining to the initial model of three strings in a plane is how the unbinding potential depth U_c depends on q if one keeps $K_1 = K_3$ fixed. In the continuum limit, the unbinding potential expressed as the rescaled potential strength v_c as defined after (26) is independent of all parameters. Assuming that it is also independent of the angle θ (as suggested above), we can write[13]

$$v_c \equiv \frac{2d^2V_c^\circ}{T^2} = \frac{2V_c^\circ K_1(l^\circ)^2}{(q+1)T^2} = \frac{\pi^2}{4}, \tag{71}$$

where we used (11) and (12) with $K_1 = K_3$. For the critical potential strength V_c°, this implies

$$V_c^\circ = (q+1)\pi^2T^2/8K_1(l^\circ)^2. \tag{72}$$

For $q = 0$, we obtain the result already known from the case of two strings. For fixed $K_1 = K_3$, the critical potential increases linearly with $q = K_1/K_2$. This effect is due to the fluctuations of the inner string, which are greatly enhanced with decreasing line tension K_2. They drive the outer strings apart, which increases the critical potential strength V_c.

5.3 ASYMPTOTIC DATA ANALYSIS. — Next, we will introduce a very effective method of analyzing our data as one approaches the unbinding transition. Consider the difference function

$$\Xi\,[F(U),\gamma'] \equiv \frac{F(U+\Delta U)^{-1/\gamma'} - F(U)^{-1/\gamma'}}{\Delta U} \tag{73}$$

Assuming that the function $F(U)$ is of the form

$$F(U) \approx a\,(U - U_c)^{-\gamma} \tag{74}$$

we obtain for small ΔU

$$\Xi \approx \frac{\gamma}{\gamma'}\,(U - U_c)^{\gamma/\gamma'-1}\,a^{-1/\gamma'} \tag{75}$$

For $\gamma/\gamma' = 1$ this expression reduces to $\Xi \approx a^{-1/\gamma'}$, which is a constant. For $\gamma/\gamma' < 1$, Ξ diverges as U tends towards U_c; for $\gamma/\gamma' > 1$, Ξ approaches zero with infinite slope as U tends towards U_c. It transpires that the difference function Ξ is a very useful tool for determining effective critical exponents, since for $\gamma = \gamma'$ the parameter U_c drops out. The existence of crossover effects in the effective exponents on the approach to U_c can be inferred from the behavior of the difference function plotted as a function of U: if the curvature of Ξ is positive and negative, one has $\gamma < \gamma'$ and $\gamma > \gamma'$, respectively.

In figures 5b and 6b we show the difference function Ξ for the angles $\theta = \pi/2$ and $\theta = 2\arctan(1/8)$, respectively. The differences are always calculated between nearest neighbor data pairs. Open symbols denote results for $\gamma' = 1$; in figure 5a, the difference functions using $\langle l \rangle$ (circles) and using $\xi_\perp$ (squares) are straight lines over the accessible range, signaling that indeed $\psi = \nu_\perp = 1$. In figure 6b, the difference functions for $\gamma' = 1$ diverge as $U - U_c$ goes to zero; this indicates that the effective exponents are smaller than unity. The closed

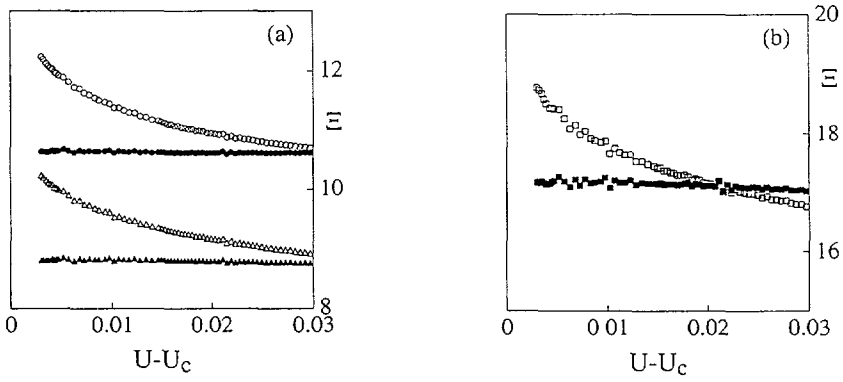

Fig. 10. — Transfer matrix results for the difference function Ξ of (a) $\langle l^2 \rangle$ (circles), $\langle l^2 \rangle^{1/2}$ (triangles), and (b) $\xi_\perp$ (squares). Shown are data with $\gamma' = 1$ (open symbols) and $\gamma' = 0.94$ (closed symbols); thus, $\psi = \nu_\perp = 0.94$ over the whole range considered here.

symbols denote $\Xi[\langle l \rangle, \psi]$ (circles) and $\Xi[\xi_\perp, \nu_\perp]$ (squares), with the effective exponents taken to be $\psi = 0.71$ and $\nu_\perp = 0.71$ as obtained in subsection 5.1. Again we obtain straight lines, signaling that there is no systematic trend in the data.

In figure 10 we present data for the angle $\theta = \pi/3$ obtained from a discretization on a hexagonal lattice using 320400 sites [21]. Values of $U - U_c$ vary by more than a decade and data for $\langle l \rangle$ range from 3 to 30. This calculation corresponds to the case of three identical strings. Data for $\Xi[\langle l \rangle, \gamma' = 1]$ (open circles) and $\Xi[\langle l^2 \rangle^{1/2}, \gamma' = 1]$ (open triangles), shown in figure 10a, and for $\Xi[\xi_\perp, \gamma' = 1]$ (open squares), shown in figure 10b, diverge as $U - U_c$ vanishes; choosing $\gamma' = 0.94$ (filled symbols) the data scale rather nicely over the whole range. These values for ψ and $\nu_\perp$ agree satisfactorily with the values obtained from an interpolation of the results shown in figure 7.

Thus, from a numerical point of view, no crossover in the data could be detected. Instead, the results indicate that $\psi < 1$ over the numerically accessible range as soon as the angle $\theta < \pi/2$. This is especially true for the case of three identical strings with $\theta = \pi/3$, where we systematically searched for such a crossover by going to very large values of $< l >$.

6. Monte Carlo simulation.

In order to check our results with a second, independent method, we performed an extensive Monte Carlo simulation of the system defined by the Hamiltonian (50) with $q = 1$, simulating three strings with identical line tensions. The range of the reduced interactions was taken to be $z^\circ = \sqrt{5/100}$ and the displacement fields z_1 and z_2 were treated as continuous variables. The length of the string was 500 in units of the lattice constant and periodic boundary conditions were used in the x-direction. The program code was fully vectorized. The moments of $\langle l \rangle$ were calculated as in the last section. However, the parallel correlation length $\xi_\parallel$ had to be determined in a different way (see Appendix C).

Using the obtained values for the parallel correlation length, we found that the length of the string must exceed the parallel correlation length by about a factor of fifty to ensure selfaveraging. We usually performed 10^7 Monte Carlo steps at a given potential value. The variance of the data was always smaller than 5 per cent.

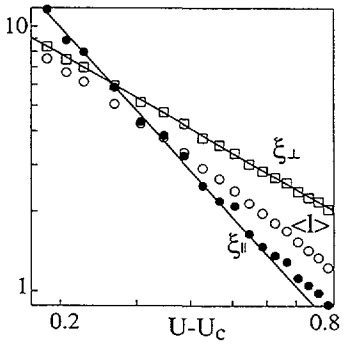

Fig. 11. — Monte Carlo results for $q = 1$. The perpendicular correlation length (open squares) diverges with the exponent $\nu_\perp = 0.93 \pm 0.05$, the parallel correlation length (closed circles) diverges with $\nu_\parallel = 1.8 \pm 0.2$. The mean separation $\langle l \rangle$ (open circles) scales as the perpendicular correlation length sufficiently close to the transition.

In figure 11 we show data for the perpendicular correlation length $\xi_\perp$ (open squares), for the parallel correlation length $\xi_\parallel$ (filled circles), and for the mean separation $\langle l \rangle$ (open circles). It is observed that the scaling relation $\xi_\perp \sim \langle l \rangle$ holds well for higher values of the mean separation. We fitted the perpendicular correlation length to a power law, yielding $U_c = 1.5733$ and the exponent $\nu_\perp = 0.93 \pm 0.05$. The mean separation does not scale as nicely and yields a somewhat higher exponent. The longitudinal correlation length yields an exponent of $\nu_\parallel = 1.8 \pm 0.2$. This yields $\zeta = 0.52 \pm 0.06$, which is to be compared with the expected value of $\zeta = 1/2$. We included this measured exponent value in figure 7 (filled square), thus confirming the transfer matrix results within our error bars.

7. Transfer matrix results for asymmetric bundles.

Now we turn to the asymmetric case with $K_1 \neq K_3$, which contains the limits $K_1 = \infty$ and $K_3 = \infty$. Inspection of the orthogonal transformation introduced in section 2 shows that the three line tensions enter the formulas for the angle θ and for the ratio of the thicknesses of the potential strips only in the form of the two ratios $q_1 = K_1/K_2$ and $q_3 = K_3/K_2$, see figure 1 and the relations (10) and (14).

In figure 12 we mapped out all different combinations of q_1 and q_3 in the plane of the angle θ and the ratio of the widths of the potential strips, d_{12}/d_{23}. Using the rescaled variables Q_1 and Q_3, defined by

$$Q_1 \equiv \frac{q_1}{q_1 + 1} = \frac{1}{1 + K_2/K_1}, \tag{76}$$

$$Q_3 \equiv \frac{q_3}{q_3 + 1} = \frac{1}{1 + K_2/K_3}, \tag{77}$$

the linear horizontal and vertical axes of the mapping are given by $Q_3/(Q_1 + Q_3)$ and $Q_1 Q_3$, respectively. The connection between the variables Q_1 and Q_3 representing the line tensions and the variables θ and d_{12}/d_{23} determining the Schrödinger problem is given by

$$\frac{Q_3}{Q_1 + Q_3} = \frac{1}{(d_{12}/d_{23})^2 + 1} \tag{78}$$

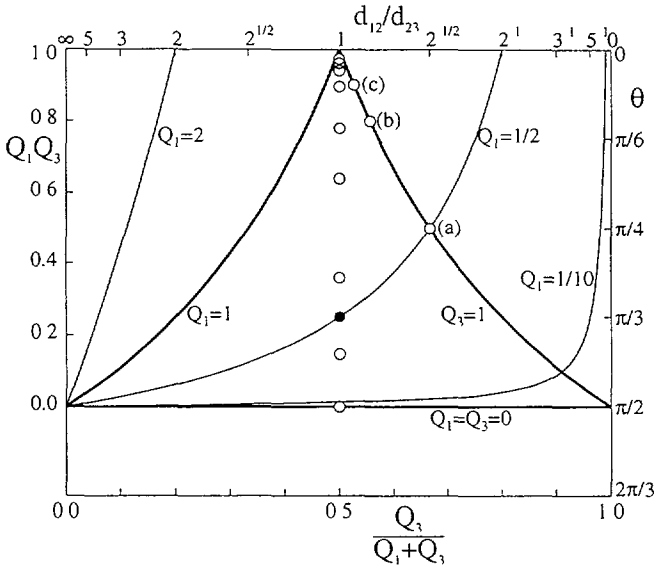

Fig. 12. — Parameter space for a string in a (1+2)-dimensional wedge with angle θ and ratio d_{12}/d_{23} of the ranges of the potential wells; see figure 1. The various lines denote lines of constant q_1 or q_3. The open and closed circles denote transfer matrix and Monte Carlo calculations, respectively. The bold lines with $Q_1 = 1$, $Q_1 = Q_3 = 0$, and $Q_3 = 1$ denote the limiting cases for three strings in two dimensions corresponding to $K_1 = \infty$, $K_2 = \infty$, and $K_3 = \infty$, respectively. The vertical line with $d_{12}/d_{23} = 1$ denotes the symmetric bundle with $K_1 = K_3$ for which the three strings unbind simultaneously. Away from this line, the unbinding process occurs in two successive transitions.

and

$$Q_1 Q_3 = \cos^2\theta, \tag{79}$$

for $V_{12}^{\circ} = V_{23}^{\circ}$ and $L_{12}^{\circ} = L_{23}^{\circ}$.

The various lines in figure 12 denote lines of constant q_1 or q_3. The three bold lines denote $q_1 = \infty$ ($Q_1 = 1$), $q_3 = \infty$ ($Q_3 = 1$), and $q_1 = q_3 = 0$ ($Q_1 = Q_3 = 0$). They correspond to the physical cases where the first string, the third string, and the string in the middle is a hard wall, respectively.

It is important to note that only the region of the parameter space inside the three bold lines is accessible starting from three strings in a plane described by Hamiltonian (5). To leave this domain of the parameter space, one would have to tune one of the line tensions to a negative value, which does not correspond to a physical situation.

Nevertheless, the region outside the bold lines constitutes a well-defined physical problem, even though it does not correspond to three strings in a plane: it represents a string in a wedge with variable angle θ and potential wells at the edges with variable thickness ratio d_{12}/d_{23}. Indeed, the bold lines (the boundaries of the physically accessible region for the unbinding of three strings in two dimensions) are by no means singular in this more general unbinding problem of one string in an attractive wedge in $d = 1 + 2$.

The values for which transfer matrix (TM) calculations have been performed are denoted by open circles, the Monte Carlo simulation is denoted by a closed circle. Most of the TM calculations have been performed for the symmetric case, i.e., on the vertical line $d_{12}/d_{23} = 1$,

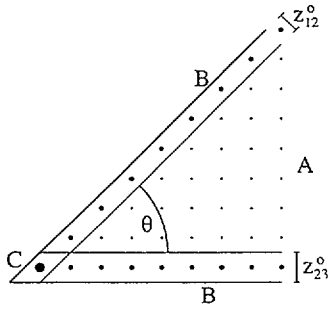

Fig. 13

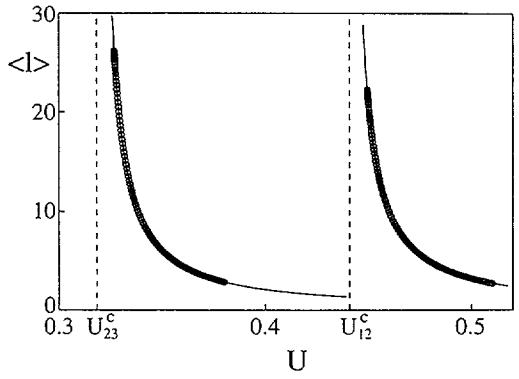

Fig. 14

Fig. 13. — Discretization used for the asymmetric bundle with $K_3 = \infty$ and $K_1 = K_2$, corresponding to (a) in figure 12. The angle of the wedge is $\theta = \pi/4$, the ratio of the widths of the two potential strips is $z^o_{12}/z^o_{23} = 2^{-1/2}$. The three regions A, B, and C correspond to regions of different potential depth as in figure 2.

Fig. 14. — Two successive unbinding transitions for two identical strings at a hard wall. The two string separations $\langle l_{12} \rangle$ and $\langle l_{23} \rangle$ diverge at different potential depths U^c_{12} and U^c_{23}. The data are fitted to a power law yielding the exponents $\psi_{12} = 1.01 \pm 0.01$ and $\psi_{23} = 1.1 \pm 0.1$.

as described in the previous section.

The straight horizontal bold line in figure 12 represents all systems with $K_2 = \infty$, corresponding to the inner string being a rigid wall. In this case, the problem separates into two, exactly solvable unbinding problems. As a consequence, the two outer strings unbind separately (at different temperatures or potential strengths) as soon as $K_1/K_3 \neq 1$. To be precise, denote the two critical potential depths at which the upper string and the lower string unbind from the rigid wall by U^c_{12} and U^c_{23}, respectively. On the bold line, i.e., for $K_2 = \infty$, the ratio of the two critical potentials is then given by

$$\frac{U^c_{23}}{U^c_{12}} = \frac{d^2_{12}}{d^2_{23}} \tag{80}$$

in the continuum limit. Only for the symmetric case with $d_{12}/d_{23} = 1$, the two unbinding transitions occur simultaneously.

Three calculations have been performed for the case of two strings unbinding from a rigid wall with $K_3 = \infty$, denoted by (a), (b), and (c) in figure 12. The parameter values are:

$$(a) \quad q_3 = \infty, \ q_1 = 1, \ \theta = \pi/4, \qquad d_{12}/d_{23} = 1/\sqrt{2}, \tag{81}$$

$$(b) \quad q_3 = \infty, \ q_1 = 4, \ \theta = \arctan(1/2), \ d_{12}/d_{23} = 2/\sqrt{5}, \tag{82}$$

$$(c) \quad q_3 = \infty, \ q_1 = 9, \ \theta = \arctan(1/3), \ d_{12}/d_{23} = 3/\sqrt{10}. \tag{83}$$

The discretization of the case (a) is given in figure 13. In all these asymmetric cases, we observed two distinct unbinding transitions. For the case (a), the measured exponents are

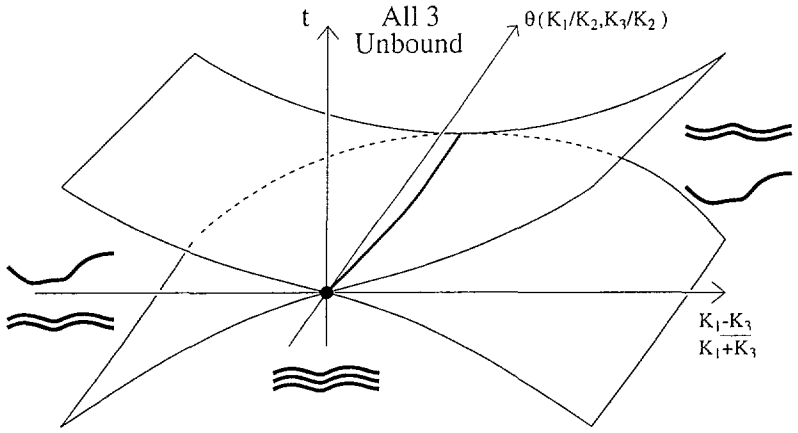

Fig. 15. — Schematic phase diagram for the unbinding of three strings with general line tensions, interacting via short-ranged potentials. The coordinates $(K_1 - K_3)/(K_1 + K_3)$, θ, and t describe the bundle asymmetry, the wedge angle, and the reduced temperature, respectively. For large t, i.e., for high temperatures or low potential depths, the three strings are unbound; conversely, for small t, i.e., for low temperatures or high potential depths, the three strings are tightly bound together. In the symmetry plane, for $(K_1 - K_3)/(K_1 + K_3) = 0$ (which contains the filled circle), the three strings unbind simultaneously at a multicritical point which belongs to the bold solid line. As one leaves this symmetry plane, the unbinding proceeds via two separate unbinding transitions as one crosses the two wings, governed by universal critical exponents. Between the two wings, one is left with a bound pair of two strings. The plane with $\theta = \pi/2$ (which also contains the filled circle) corresponds to the middle string being a rigid wall, in which case the problem is exactly solvable.

$\psi_{12} = 1.01 \pm 0.01$ for the unbinding at $U_{12}^c = 0.44124$ and $\psi_{23} = 1.1 \pm 0.1$ for the second unbinding at $U_{23}^c = 0.31634$. Data for $\langle l_{12} \rangle$ and $\langle l_{23} \rangle$ together with the fitted curves are shown in figure 14. A finite size scaling analysis indicates that the second exponent tends towards unity with increasing size of the system and with closer approach to the transition. Consequently, we are led to the conclusion that the unbinding transition proceeds via two separate transitions not only for the case $\theta = \pi/2$, but for all values of θ as soon as $d_{12}/d_{23} \neq 1$. The transitions are then characterized by the universal exponent $\psi = 1$.

Based on these results, the vertical line which corresponds to the symmetric case ($K_1 = K_3$) in figure 12 is identified to be a line of multicritical points; on this line the three strings unbind simultaneously with critical exponents which seem to vary along this line. If one steps off this line, the three strings unbind separately with the universal exponent $\psi = 1$. This is shown schematically in figure 15. The horizontal axis measures the asymmetry $(K_1 - K_3)/(K_1 + K_3)$, the vertical axis measures the ratio of temperature and potential depth in units of t as given by (27), the third axis measures the relative tension of the inner string in units of the angle θ. At the point denoted by the filled circle, the tension of the inner string is infinitely high. The plane with constant $\theta = \pi/2$, where we recover the behavior of two decoupled strings and which contains this point, contains two exactly known transition lines, which meet at this point. In this plane, the multicritical point is decoupled, meaning that the critical behavior at this point is not different from the behavior off the point. At high temperatures and large t, all three strings are unbound, at low temperatures and small values of t, they are bound together. At

intermediate temperatures and off the symmetry line $(K_1 - K_3)/(K_1 + K_3) = 0$, we obtain a situation where just one string is unbound, whereas the other two still form a bound pair. This represents the simplest phase diagram which is consistent with our data. Note that, following the discussion in subsection 5.2, the reduced transition temperature t seems not to depend on the angle θ, and the multicritical line in figure 15 is likely to be straight and horizontal in the continuum limit.

As one softens the inner string, the angle θ decreases and one moves back into the diagram shown in figure 15. As described in section 5, our calculations for the symmetric case give θ-dependent critical behavior for the accessible range of length scales. If this θ-dependence applies to the asymptotic critical behavior, the multicritical points on the line are coupled. On the other hand, the unbinding transitions on the four wings in figure 15 are still governed by universal critical exponents and meet in the plane defined by the symmetry $K_1 = K_3$. One then expects crossover lines changing the critical behavior from universal to non-universal, depending on the distance from the transition. However, the four regions corresponding to different physical states of the three strings still meet at this line.

8. Conclusions.

We considered the general problem of the unbinding of three strings with different string tensions in two dimensions. The interaction potential was short-ranged and of a square-well form.

For the symmetric case, where the tensions of the two outer strings are identical, the three strings unbind simultaneously. If the inner string corresponds to a rigid wall, the two outer strings are decoupled and the critical exponent ψ has the universal value $\psi = 1$, as confirmed by our calculation. As soon as one softens the inner string, the value for ψ as determined in the transfer matrix calculation changes in a continuous fashion. This behavior is analogous to the unbinding of two strings in the presence of a repulsive potential which goes as $V(l) \sim 1/l^2$. This analogy is expected from a simple scaling picture, since the spatial confinement of the inner string due to the presence of the two outer strings at distance l leads to an entropically generated loss in free energy of the identical functional form.

Based on our numerical data, we estimate that one stays in the regime of continuous unbinding transitions, i.e., the so-called subregime (B), at least until the inner string becomes about 130 times more flexible than the outer strings.

The critical potential depth V_c^o increases linearly with the tension ratio $q = K_1/K_2 = K_3/K_2$ for fixed $K_1 = K_3$. However, we estimate that three identical strings unbind at the same potential strength as two identical strings.

As soon as the up-down symmetry of the string bundle is broken and $K_1 \neq K_3$, the unbinding proceeds via two separate transitions, which exhibit the same critical behavior as the unbinding transition of two strings. The symmetry line is thus revealed to be a line of multicritical points.

Finally, the effective Hamiltonian as given by (6) can also be studied by functional renormalization group methods.[1] For infinitesimal rescaling factor $b \approx 1 + \Delta t$, one obtains

$$\frac{1}{\zeta}\frac{\partial U}{\partial t} = \tau U + y_\alpha \partial_\alpha U + \ln \det(\delta_{\alpha\beta} + \partial_\alpha \partial_\beta U), \tag{84}$$

where the two-dimensional potential $U(\mathbf{y})$ is a rescaled superposition of the mutual interactions in (6). For strings in two dimensions one has $\zeta = 1/2$ and $\tau = 2$. The flow equation (84) also applies to fluid membranes in three dimensions with $\zeta = 1$ and $\tau = 2$. Since $\tau = 2$ in both cases, the fixed points, defined by $\partial U/\partial t = 0$, are identical, and the critical exponents are related in a trivial way. Thus our results obtained for three strings should also be applicable to three

interacting membranes, as confirmed by recent MC simulations of three fluid membranes [6, 21]. Experimentally, it has been observed that there is no or little dependence of the unbinding temperature of a stack of membranes on the actual number of membranes involved.[4] This can be understood by using the analogy between strings and membranes (84) and our results for the critical potential strength of two and three interacting strings, where the same behavior is observed.

Very recently, two mean-field type calculations for the simultaneous unbinding of a stack of identical membranes have been described,[9, 10] which predict *universal* critical behavior, in contrast to the results presented here.

In addition, the problem of N identical strings ($N > 2$) has been studied via an approximate mapping onto a quantum spin chain [11], and has been solved analytically in the continuum limit for infinitesimally small potential ranges [12], which also leads to N-independent critical behavior.

Thus, it is conceivable that we have not determined the asymptotic critical behavior by our numerical iterations, but have observed a pronounced crossover regime. In the latter case, the critical exponents determined here, see figure 7, would represent effective exponents which applied only to a certain range of length scales. Since the range of scales studied in our work is rather large, however, these effective exponents would also apply to the accessible behavior of real systems governed by short-ranged forces.

Useful discussions with Ted W. Burkhardt, Wolfgang Helfrich, Christin Hiergeist, and Michael Lässig are gratefully acknowledged.

Appendix A.

Orthogonal transformation.

First, one absorbs the line tension parameters into the displacement fields by the following coordinate transformation:

$$y_1' = \sqrt{K_1}\, l_1 \ , \ y_2' = \sqrt{K_2}\, l_2 \ , \ y_3' = \sqrt{K_3}\, l_3. \tag{A.1}$$

After a rotation of the coordinate system the potential energy in Hamiltonian (5) depends on two displacement fields only. The transformation $(y_1, y_2, y_3) = \mathcal{O}[(y_1', y_2', y_3')]$ is explicitly defined by the matrix

$$\mathcal{O} = \begin{pmatrix} \dfrac{(K_1)^{-1/2}}{b} & -\dfrac{(K_2)^{-1/2}}{b} & 0 \\ \dfrac{(K_3/K_2)^{1/2}}{ab} & \dfrac{(K_3/K_1)^{1/2}}{ab} & -\dfrac{b(K_1K_2)^{1/2}}{a} \\ \dfrac{(K_1)^{1/2}}{a} & \dfrac{(K_2)^{1/2}}{a} & \dfrac{(K_3)^{1/2}}{a} \end{pmatrix}, \tag{A.2}$$

with $a \equiv (K_1 + K_2 + K_3)^{1/2}$, $b \equiv (1/K_1 + 1/K_2)^{1/2}$ and $\det(\mathcal{O}) = 1$ and $\mathcal{O}^{-1} = \mathcal{O}^{\mathrm{T}}$

String separations appearing in the Hamiltonian (5) can now be calculated as follows:

$$l_1 - l_2 = \frac{y_1'}{\sqrt{K_1}} - \frac{y_2'}{\sqrt{K_2}} = \left(\frac{1}{K_1} + \frac{1}{K_2}\right)^{\frac{1}{2}} y_1, \tag{A.3}$$

$$l_2 - l_3 = \frac{y_2'}{\sqrt{K_2}} - \frac{y_3'}{\sqrt{K_3}} = \left(\frac{1}{K_2} + \frac{1}{K_3}\right)^{\frac{1}{2}} (y_2 \sin\theta - y_1 \cos\theta), \tag{A.4}$$

where

$$\sin\theta = \left(\frac{K_2(K_1+K_2+K_3)}{(K_1+K_2)(K_2+K_3)}\right)^{\frac{1}{2}}, \tag{A.5}$$

$$\cos\theta = \left(\frac{K_1K_3}{(K_1+K_2)(K_2+K_3)}\right)^{\frac{1}{2}}. \tag{A.6}$$

The potential energy does not depend on the center-of-mass coordinate $y_3 = (K_1l_1 + K_2l_2 + K_3l_3)/a$ which diffuses freely and can be omitted from the Hamiltonian.

Appendix B.

Exact solution in one dimension.

The discretized one-dimensional Hamiltonian is constructed in analogy to (49) and (50) and given by

$$\mathcal{H}\{z_i\}/T = \sum_i \left[\frac{1}{2}(z_i - z_{i+1})^2 + \hat{V}(z_{i+1})\right] \tag{B.1}$$

with

$$\hat{V}(z) = -U \quad \text{for} \quad 0 < z < z^\circ. \tag{B.2}$$

It derives from a system of two strings after subtraction of the center-of-mass coordinate. The range of the attractive potential is measured in multiples of the lattice constant Δz and given by $z^\circ = n\Delta z$. For the case $n = 1$, i.e., where the attractive potential extends over one lattice site, the problem has been solved exactly [22]. Here, we extend the results for U_c to the cases $n = 2, 3$. First, one defines

$$B \equiv \mathrm{e}^{-U} \quad \text{and} \quad R \equiv \mathrm{e}^{-(\Delta z)^2/2} \tag{B.3}$$

The critical potential can be expressed for general n as

$$B_c = \frac{1 + x(n)R}{1 + 2R} \tag{B.4}$$

with

$$x(n = 1) = 1 \tag{B.5}$$

in agreement with the known result [22],

$$x(n = 2) = \frac{1}{2} + \frac{\sqrt{5}}{2} \simeq 1.618, \tag{B.6}$$

$$x(n = 3) = \frac{1}{3} + \frac{2\sqrt{7}}{3}\cos\left[\frac{\arccos\left(\frac{1}{2\sqrt{7}}\right)}{3} - \frac{\pi}{3}\right] \simeq 1.802. \tag{B.7}$$

For infinite potential range, one expects $x(n = \infty) = 2$. Setting the lattice constant $\Delta z = 1$ as was done in the numerical analysis, we obtain for the critical potential strengths $U_c(z^\circ = 1) \simeq 0.3203$, $U_c(z^\circ = 2) \simeq 0.1106$, and $U_c(z^\circ = 3) \simeq 0.0558$. These exact results are denoted in figure 9 as crosses; the corresponding numerical results, obtained for a system using 1000 discretization sites, are denoted by filled circles.

Appendix C.

Determination of the parallel correlation length.

Consider the correlation function $C(z)$, which is defined as

$$C(z) = \langle l(z_o + z) l(z_o) \rangle - \langle l(z_o + z) \rangle \langle l(z_o) \rangle, \tag{C.1}$$

the brackets denoting an average over time only. Averaging over the system does not change the function, since the system is translationally invariant:

$$C(z) = \int \frac{dz_o}{L} \langle l(z_o + z) l(z_o) \rangle - \langle l(z_o + z) \rangle \langle l(z_o) \rangle, \tag{C.2}$$

where L is the length of the system. The fourier transformed of this function for $q = 0$ is (in the continuum limit)

$$\tilde{C}(q = 0) = \int \frac{dz_o}{L} \int dz \langle l(z_o + z) l(z_o) \rangle - \langle l(z_o + z) \rangle \langle l(z_o) \rangle. \tag{C.3}$$

Using the notation $\bar{l} = \int dz l(z)$ we arrive at the following equation:

$$\tilde{C}(q = 0) = \frac{\langle (\bar{l})^2 \rangle - \langle \bar{l} \rangle^2}{L} \tag{C.4}$$

On the other hand, the parallel correlation length can be defined to be $\xi_{\|} = \sqrt{(K/T)\tilde{C}(q = 0)}$, so that we get the final expression

$$\xi_{\|} = \sqrt{\frac{K(\langle (\bar{l})^2 \rangle - \langle \bar{l} \rangle^2)}{LT}}. \tag{C.5}$$

References

[1] Lipowsky R., *Phys. Scr.* **T 29** (1989) 259;
Forgacs G., Lipowsky R., and Nieuwenhuizen Th.M., Phase Transitions and Critical Phenomena, C. Domb and J. Lebowitz Eds. (Academic, London, 1991) Vol. 14.

[2] A review of wetting transitions in two and three dimensions is provided by Fisher M.E., *J. Chem. Soc. Faraday Trans. 2* **82** (1986) 1569.

[3] Lipowsky R., Nature (London) **349** (1991) 475; *Physica* A **194** (1993) 114.

[4] Helfrich W. and Mutz M., *Random Fluctuations and Growth*, H.E. Stanley and N. Ostrowsky Eds. (Kluwer, Dordrecht, 1988);
Mutz M. and Helfrich W., *Phys. Rev. Lett* **62** (1989) 2881.

[5] Fisher M.E. and Gelfand M., *J. Stat. Phys.* **53** (1988) 175.

[6] Cook-Röder J. and Lipowsky R., *Europhys. Lett.* **18** (1992) 433.

[7] Lipowsky R. and Zielinska B., *Phys. Rev. Lett.* **62** (1989) 1572.

[8] Netz R.R. and Lipowsky R., *Phys. Rev. E* **47** (1993) 3039.

[9] Milner S.T. and Roux D., *J. Phys. I France* **2** (1992) 1741.

[10] Helfrich W., *J. Phys. II France* **3** (1993) 385.

[11] Burkhardt T.W. and Schlottmann P., *J. Phys. A* **26** (1993) L501.
For a lucid discussion of the methods used (and its limitations) see Burkhardt T.W. and Schlottmann P., *Z. Phys. B* **54** (1984) 151.

[12] Hiergeist C., Lässig M. and Lipowsky R. (to be published).

[13] Lipowsky R. and Nieuwenhuizen T.M., *J. Phys. A* **21** (1988) L89.

[14] McGuire J.B. and Hurst C.A., *J. Math. Phys.* **13** (1972) 1595.

[15] Balian R. and Toulouse G., *Ann. Phys.* **83** (1974) 28.

[16] Lipowsky R., *Europhys. Lett.* **15** (1991) 703.

[17] Lipowsky R., Grotehans S. and Schmidt G.J.O., *Mat. Res. Soc. Symp. Proc.* **237** (1992) 11.

[18] Note that Eq.(4.8) in [5] should read as $m_c(V_o) = 2(\psi_3(b_y) - 2)$.

[19] W.H. Press, B.P. Flannery, S.A. Teukolsky and W.T. Vetterling Eds., Numerical Recipes: The Art of Scientific Computing, 1989, p. 523.

[20] The free energy of the lowest scattering state, f_o, for an infinite system can be calculated from (61) using $\mathcal{N}_o = 1 + 4e^{-(\Delta z)^2/2} + 4e^{-(\Delta z)^2}$

[21] Netz R.R. and Lipowsky R., to be published.

[22] Chui S.T. and Weeks J.D., *Phys. Rev. B* **23** (1981) 2438.